Available online at www.sciencedirect.com
SCIENCE DIRECT®
International Journal of Thermal Sciences 43 (2004) 769–777
International Journal of Thermal Sciences
www.elsevier.com/locate/ijts

Double-diffusive convective modes and induced microstructure localisation during solidification of binary alloys

Haik Jamgotchian *, Henri Nguyen Thi, Nathalie Bergeon, Bernard Billia

Laboratoire L2MP, UMR 6137, faculté des sciences et techniques de St Jérôme, case 142, 13397 Marseille cedex 20, France

Received 25 August 2003; received in revised form 7 January 2004; accepted 24 February 2004

Available online 17 June 2004

Abstract

We analysed the coupling of convection and solid-liquid interface morphology during upward Bridgman solidification of both transparent and metallic alloys in a cylinder. Localised microstructures are observed for typical alloys but not for lead-30 wt% thallium. This difference is quantitatively explained from phase diagrams and from the more general form of constitutional supercooling criterion, extended for non-dilute alloys. Even if the convection induces a lateral concentration gradient, there is not any lateral gradient on the level of morphological instability and there is not any propagation front of morphological instability for lead-30 wt% thallium alloy. In solidification experiments, convection can be generated by either radial thermal gradient or solute axial gradient. The formation and dynamics of double-diffusive convective pattern is analysed during the transient and different thermal radial gradient conditions.

Keywords: Directional solidification; Morphological instability; Double-diffusive instability; Localised microstructure; Initial transient; Thermal radial gradient

1. Introduction

Materials properties strongly depend on non-homogeneity left in the solid during processing. An important point to clarify in the solidification process is the role of convection on macrosegregation and on microstructure selection. Interface morphology is directly related to the radial micro and macro segregation. Thus, an important point in solidification is the coupling effect of different instabilities at different length scales.

The coupling between fluid flow and solidification has been the subject of a great deal of experimental, theoretical and numerical works. For the laterally infinite medium Coriell et al. first tackled the linear stability analysis of coupling double-diffusive and morphological instability analysis [1]. They numerically calculated the domains of morphological and convective instabilities. Then many authors enlarged the study such as by neglecting the thermal expansion on density for obtaining a more analytical solution [2] or by introducing the density differences between liquid and solid [3], or by looking at the effect of lateral confinement [4,5].

The effect of convection on morphological instability is another aspect of the problem. Indeed, the level of convection changes the threshold of morphological instability. For the majority of alloys ($K < 1$), instability begins later than for pure diffusive case [6–8]. The case of the effect of pre-existing convective cellular pattern on the morphological instability is studied by Chen and Davis [9]. They predict a localised microstructure induced by convective pattern, which recently received experimental confirmation [10]. However, this result is in contradistinction with previous study on lead-30% thallium alloys, where localised microstructure is not observed [11,12]. The question is why convective pattern on lead-30% thallium alloy does not give localised microstructure?

When the solidification experiments are far above the thresholds of instability, the determination of the levels of morphological and convective instabilities is a real problem. In fact they are function of time and depend on initial conditions, i.e., on initial transient. Moreover, the situation is fur-

* Corresponding author. Fax: +33-4-91-28-87-75.
E-mail addresses: haik@L2MP.u-3mrs.fr (H. Jamgotchian), nthenri@L2MP.u-3mrs.fr (H.N. Thi), bergeon@L2MP.u-3mrs.fr (N. Bergeon), bernard.billia@L2MP.fr (B. Billia).

1290-0729/$ – see front matter
doi:10.1016/j.ijthermalsci.2004.02.017

Nomenclature

C	concentration in the liquid	wt%
C_i	interface concentration	wt%
D	solute diffusion coefficient in the liquid	$m^2 \cdot s^{-1}$
G	thermal gradient in the liquid at the interface	$K \cdot m^{-1}$
G_s	solute gradient in the liquid at the interface	$wt\% \cdot m^{-1}$
g	gravitational acceleration, $= 9.81$	$m \cdot s^{-2}$
K	partition coefficient, $= \frac{C_i^s}{C_i^l}$	
k	thermal conductivity	$J \cdot m^{-1} \cdot K^{-1} \cdot s^{-1}$
L_s	thickness of solute boundary layer	m
m	liquidus slope	$K \cdot wt\%^{-1}$
Pr	Prandtl number, $= \frac{\nu \rho c_p}{k}$	
Ra_s	solute Rayleigh number, $= \frac{\beta_s g G_s L_s^4}{\nu D}$	
V	growth velocity	$m \cdot s^{-1}$
V_p	pulling velocity	$m \cdot s^{-1}$
z	growth axis	m

Greek symbols

β_s	solutal expansion coefficient in the melt, $= -\frac{1}{\rho}(\frac{\partial \rho}{\partial C})_T$	$wt\%^{-1}$
β	thermal expansion coefficient in the melt, $= -\frac{1}{\rho}(\frac{\partial \rho}{\partial T})_C$	K^{-1}
ΔT	temperature difference between liquidus and solidus	K
δT	temperature variation	K
δC	concentration variation	wt%
$\delta \rho$	density variation	$kg \cdot m^{-3}$
ν	kinematic viscosity	$m^2 \cdot s^{-1}$
ρ	density	$kg \cdot m^{-3}$
ϕ	crucible diameter	m

Subscripts

0	reference state
s	solute contribution

Superscripts

c	critical value
l	liquid phase
s	solid phase

ther complicated because thermal radial gradient also contributes to both convective and morphological instabilities. Each experimental procedure is specific by itself and needs a specific analysis in order to explain the observed phenomena. A non-linear time dependent approach for a system far from equilibrium is needed to explain the observed dynamics of microstructure and macrostructure patterns. Other questions deal with the effects of radial thermal gradient and transient phenomena on the double-diffusive convective pattern.

In this paper, the coupling effect of convection and morphological instability is described for different experimental configurations. Three series of experiments are compared in order to understand pattern formation in initial transient and the effect of the radial thermal convection on the double-diffusive convective pattern. The first one is in situ and in real time study of interfacial shape on succinonitrile-acetone alloys, the two others are on lead–thallium alloys for different crucible diameters. The absence of localised microstructure on the lead-30 wt% thallium alloys is explained from the shape of phase diagram. The explanation needs some generalisation of constitutional supercooling criterion, extending its application to non-dilute alloys.

2. Experiments

For dynamical study, succinonitrile–acetone alloy, equivalent to metallic alloys, is used. Experiments are done in a vertical Bridgman configuration with positive thermal gradient (upward solidification), in laboratory devices especially built for transparent 3D growth [13]. The furnaces consist of three main zones: a hot zone (in two parts), a cold zone and an adiabatic zone. In the hot zone a small thermal vertical gradient is established in order to eliminate thermal convection. During experiments the higher part is maintained at 110 °C and lower part at 100 °C. The cooler zone is maintained at 20 °C. The thermal measurement gives a vertical thermal gradient 3 $K \cdot mm^{-1}$ in the middle of the adiabatic zone. A cylindrical crucible of $\phi = 10$ mm in inner diameter is used. The growth velocity is anti-parallel to the gravity and varied from 0.5 to 2 $\mu m \cdot s^{-1}$. Experiments are performed essentially on succinonitrile-0.2 wt% acetone alloy. For this alloy the partition coefficient is constant and is equal to $K = 0.1$ (Fig. 1(a)). The solid–liquid interface is observed by three complementary optical techniques: two direct observation modes providing bright field images of the interface, one transmitted through the whole length of the sample and another one through the radial direction. A Mach–Zehnder interferometer set-up on the longitudinal direction gives the 3D shape and the position of the interface. In situ and real-time images are recorded on videotape.

Experiments on Pb–Tl alloys are carried out in vertical upward Bridgman configuration [14]. Higher zone of furnace is maintained at 650 °C and the lower zone is cooled by water circulation. Experiments are carried out for pulling velocities from 0.55 to 6.11 $\mu m \cdot s^{-1}$, which are applied anti-parallel to the gravity. Two crucible diameters $\phi = 4$ mm and $\phi = 9.5$ mm are used in order to change both thermal radial gradient and confinement, with imposed thermal axial gradient respectively of 5.5 and 4.0 $K \cdot mm^{-1}$. For these alloys

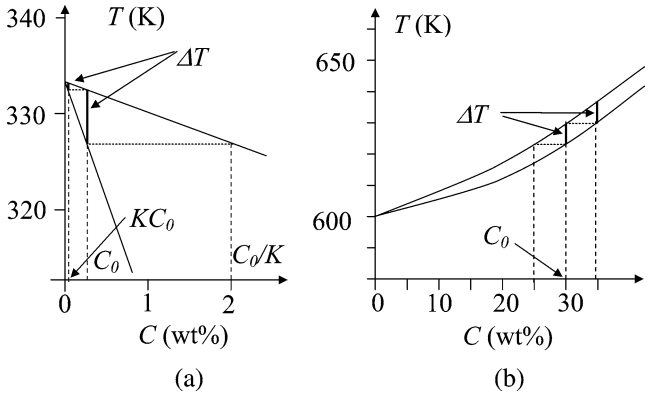

Fig. 1. Schematic presentation of phase diagram of (a) succinonitrile–acetone alloy and (b) lead–thallium alloy.

the partition coefficient is higher than 1 (Fig. 1(b)). The solidification is stopped by a quench using a flow of helium at liquid nitrogen temperature. Successive polishing-chemical etching process in interfacial region gave microstructure pattern and level curves of macroscopic shape of the interface on the transverse section.

3. Front morphologies induced by instabilities

The best understanding of the solidification process with different instabilities at different length scales asks at first to look basics of solidification process. It corresponds to the 1D steady state solidification, in purely diffusive case, with stable planar interface. This is characterised by three control parameters: initial alloy solute concentration C_0, pulling rate V_p and thermal gradient G. The solid–liquid interface is supposed in thermodynamic local equilibrium. Due to the equality of chemical potentials at the interface, the concentration in the liquid is different from that in the solid. The partition coefficient K is defined as the ratio of solid concentration to the liquid one at the interface. The resolution of the solute diffusion equation in the liquid in the reference frame attached to the interface with boundary conditions $C = C_0$ far from the interface and $C = C_0/K$ at the interface, gives the following solution for the solute concentration in the liquid:

$$C = C_0\left[1 + \frac{1-K}{K}\exp\left(-\frac{V_p}{D}z\right)\right] \tag{1}$$

where D is the diffusion coefficient and z the growth direction. Positive part of solid line in Fig. 2 represents the solute profile in steady state solidification given by Eq. (1) for an alloy $K < 1$. During alloy solidification, the solute (solvent) is rejected into the liquid at the interface, and diffuses in the liquid, which gives an exponential diffusive profile in front of the interface. Usually, the partition coefficient is smaller than one but for some alloys it is greater than one as is the case for lead–thallium alloy (Fig. 1(b)). For this reason the physical interpretation is usually done for the

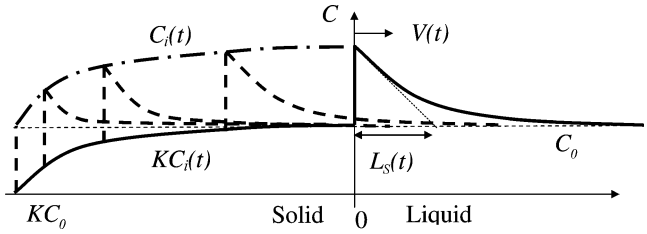

Fig. 2. Solute profile for an alloy $K < 1$. Solid line: steady state profile. Dashed lines: transient state profiles at a regular time interval. Dotted line: concentration variation in the liquid at the interface.

case $K < 1$ which will be extended for $K > 1$, by changing the solute by solvent.

The liquid in front of interface is rich in solute (solvent) that can drive some instability. Let us see the necessary conditions for morphological and hydrodynamic instabilities.

3.1. Morphological instability

For fixed C_0 and G, the interface is morphologically planar for low velocity. Increasing velocity leads to the breakdown of the planar interface for a critical velocity, V^c, and gives rise to a cellular structure. For higher velocity, the interfacial microstructure undergoes a transition into the dendritic regime with apparition of secondary arms. The breakdown of planar interface is due to the constitutional supercooling introduced by Tiller et al. [15]:

$$G < mG_s \tag{2}$$

Where G_s is solute gradient at the interface and is given by:

$$G_s = \frac{C_0(K-1)}{K}\frac{V_p}{D} \tag{3}$$

This criterion is based on the thermodynamic state of the liquid adjacent to the interface, which enters into non-equilibrium (supercooling) when growth velocity becomes higher than critical one. Later, Mullins and Sekerka have given a more accurate criterion of the stability of planar interface by a linear stability analysis [16]. They added the capillarity and the thermal gradient in the solid, which under usual growth conditions modify only slightly the constitutional supercooling criterion. The growth velocity and the concentration have destabilising effect, in contrast to the thermal axial gradient and the capillarity that have a stabilising effect. In practice, the constitutional supercooling criterion remains a good approximation, and is frequently used, in the domain of low capillarity and low anisotropy of thermal conductibility at the interface.

The morphological instability criterion is established for steady state solidification, and can be generalized for transient state. The growth velocity V varies from zero to V_p, and the interface concentration in the liquid, C_i, from C_0 to C_0/K, as shown in Fig. 2 by dotted line. According to Warren and Langer model [17], for a given instantaneous velocity V, the solute vertical gradient G_s can be calculated:

$$G_s = \frac{C_i(K-1)}{L_s} \tag{4}$$

where L_s is the thickness of solute boundary layer that varies from zero to the value of steady state of solidification, D/V_p [17]. Thus, the constitutional supercooling criterion can be written as following:

$$GL_s < C_i K m\left(1 - \frac{1}{K}\right) \tag{5a}$$

All above considerations are true in the limit of the linear approximation of phase diagram (K and m constants), thus for a dilute alloy. Fig. 1 presents the phase diagrams of succinonitrile-acetone and lead–thallium alloys. Linear approximation of phase diagram is correct for both succinonitrile–acetone and lead–thallium alloys in the domain of low concentration. However, for the higher concentrations used for lead–thallium alloys, this approximation is not valid, because K and m depend on the concentration. RHT in the inequality (5a) corresponds to the temperature difference between the liquidus and the solidus, ΔT, for a given concentration, $C_i K$, i.e., solid concentration at the interface. Thus, a more general form of constitutional supercooling criterion is the following:

$$GL_s < \Delta T \tag{5b}$$

This general form is very convenient for lead-30 wt% thallium alloy, because ΔT is independent of concentration, i.e., the liquidus is parallel to the solidus. Thus, even if solute concentration at the interface is not constant, the level of instability does not change. This is in contradistinction with the constitutional supercooling criterion for dilute alloys, where concentration at the interface is proportional to ΔT. Thus, a particular attention should be taken using constitutional supercooling criterion or Mullins–Sekerka criterion for non-dilute alloy. This fact could be of major importance for the interpretation of experimental results.

3.2. Double-diffusive instability

The axial solute gradient is intrinsic to the alloy solidification process and can be stabilising or destabilising from hydrodynamic point of view. Let us consider the density variation in the melt $\delta\rho$ as a function of temperature and concentration variations, δT, δC:

$$\delta\rho = -\rho(\beta\delta T + \beta_s \delta C) \tag{6}$$

In the growth direction z, thermal contribution is similar for both alloys: thermal gradients and thermal expansion coefficients are positive. However, solute gradient at the interface is negative for succinonitrile–acetone alloy and positive for lead–thallium alloy. This difference in solute gradients comes from the alloy characteristics, i.e., solute partition coefficient and liquidus slope: $K > 1$, $m > 0$, for lead–thallium alloy and $K < 1$, $m < 0$ for succinonitrile–acetone alloy (Table 1). As the solute expansion coefficients are reversed too, the solute contribution on the density variation is thus similar for both lead–thallium and succinonitrile–acetone alloys. The Fig. 3 schematically represents density profiles in the liquid, for both alloys. Finally, both alloys exhibit similar double-diffusive instability, i.e., the axial solute gradient has a destabilising effect into the solute diffusion layer. The Fig. 4 schematically shows the double-diffusive convective pattern and front deformation for both alloys. Convection begins into the solute diffusion layer and continues invade the stable liquid by the double-diffusion phenomena. The major difference between the two alloys is that, in the case of succinonitrile–acetone, solute accumulation occurs in depression of the interface and straight below up-going flow [10], whereas for lead–thallium alloys, this situation corresponds to the solvent accumulation [11].

Convective instability in the liquid will be assumed essentially solutal in the sense that the thermal axial contribution can be safely discarded in the linear analysis of the hydro-

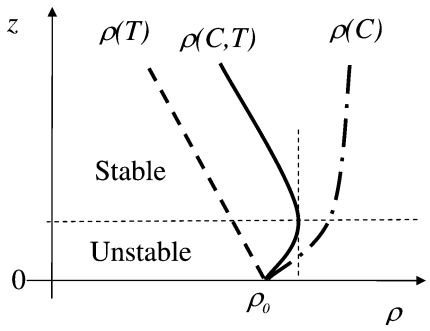

Fig. 3. Schematic presentation of density profiles (solid line) in the liquid for both succinonitrile–acetone and lead–thallium alloys. Liquid in the solute boundary layer is hydrodynamically instable. Thermal (dashed line) and solutal (dotted line) contributions of density are distinguished.

Table 1
Lead–thallium and succinonitrile–acetone alloy characteristics

	Symbol [units]	Succinonitrile–acetone	Lead–thallium
Segregation coefficient	K	0.1	≈ 1.1
Liquidus slope	m [K·wt%$^{-1}$]	-2.8	≈ 1
Liquidus–solidus temperature difference	ΔT [K]	–	2.7
Liquid kinematic viscosity	ν [m^2·s^{-1}]	2.6×10^{-6}	2.43×10^{-7}
Solute diffusivity in the melt	D [m^2·s^{-1}]	1.3×10^{-9}	2×10^{-9}
Thermal expansion coefficient in the melt	β [1·K^{-1}]	1.07×10^{-3}	1.15×10^{-4}
Solutal expansion coefficient in the melt	β_s [1·wt%$^{-1}$]	2.13×10^{-3}	-5.3×10^{-4}
Liquid thermal conductivity	k^l [J·m^{-1}·K^{-1}·s^{-1}]	0.2219	15.5
Solid thermal conductivity	k^s [J·m^{-1}·K^{-1}·s^{-1}]	0.2244	31.4
Prandtl number	Pr	17	0.02

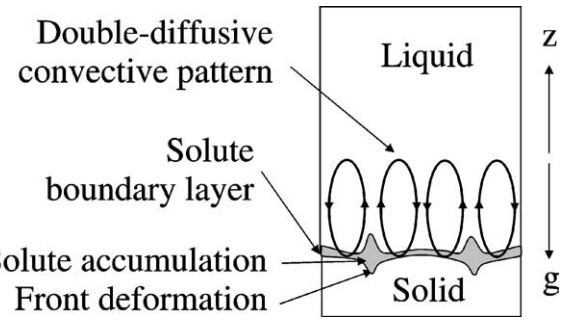

Fig. 4. Schematic representation of double-diffusive convective pattern. Ascending flow corresponds to the interface depression and solute (solvent) accumulation.

dynamic stability of quiescent melt [2,3]. In this condition fluid flow in the liquid phase depends essentially on the solutal Rayleigh number:

$$Ra_s = \frac{\beta_s g G_s L_s^4}{\nu D} \tag{7}$$

where g is gravitational acceleration, ν the kinematic viscosity. The double-diffusive instability begins when Ra_s exceeds the critical value of convective instability, $Ra_s^c \cdot Ra_s^c$ depends on lateral confinement [5], but for large crucible diameters, the value for a laterally unbounded medium ($Ra_s^c = 7.9$ for $K = 0.1$ and $Ra_s^c = 12.4$ for $K = 1.1$) can be used [18].

There is a major difficulty in the experimental determination of solutal Rayleigh number. It strongly depends on the thickness of the solute boundary layer, L_s. The convection due to the thermal radial gradient and transient effects may change considerably the thickness of solute boundary layer. In fact, as there is no instability threshold for the convection induced by thermal radial gradient, the convection could be present before the onset of double-diffusive instability, and decrease the thickness of solutal boundary layer. For this reason, in this article a more general term "convective pattern" is frequently used, which is introduced to encompass the "double-diffusive instability" or/and the "convection due to the thermal radial gradient". The thermal radial gradient depends on alloy (metallic or transparent), initial conditions and external parameters such as crucible diameter, thermal conductibility of crucible and thermal profile of furnace [19–23]. As Prandtl number depends strongly on the choice of alloy (see Table 1), the thermal radial contribution is not similar for metallic and transparent systems. In this study, we qualitatively examine the effect of thermal radial gradient on convective patterns. For this reason, we just need to know that, for metallic alloys, increasing the crucible diameter increases the contribution of the radial thermal gradient on convective pattern and in our range of growth velocity, thermal radial gradient is supposed independent of growth velocity [24]. For transparent alloys, the evacuation of latent heat of solidification is mainly done by the crucible wall due to the low thermal conductivity of the alloy compared to glass; this is of major importance as latent heat depends on growth velocity [25] and has a large variation during transient state of solidification.

In conclusion, as the value of L_s depends on the level of convection, it would not be possible to attribute any real Rayleigh number to the observations given for steady state of solidification. However, we can attribute a level of double-diffusive instability as the ratio Ra_s/Ra_s^c where Ra_s is defined for steady state solidification in purely diffusive transport case, i.e., $L_s = D/V_p$. On the other hand, during the solidification transient, where L_s varies from zero to the D/V_p, the value of Ra_s will be calculated from the Warren and Langer model [17]. The liquid in front of solid–liquid interface becomes unstable with respect to double-diffusive instability when the ratio $Ra_s/Ra_s^c > 1$.

3.3. Results and discussion

For succinonitrile–acetone alloys, the morphological instability first initiates in interface areas of high solute concentration and propagates in the direction opposite to the horizontal solute gradient. This horizontal gradient of concentration exists because of the presence of natural convection. The level of morphological instability in transient state of solidification in presence of convection does not depend only on the instantaneous growth velocity, but also on the local interface concentration (cf. Eq. (5a)). Most likely, the solute in the boundary layer adjacent to the solidification front is swept by convection and accumulated upstream. Solute gradient can be evaluated as a function of level of convection by using the boundary layer approach proposed by Ostrogorsky and Müller [26,27]. For a given instantaneous velocity V, the critical interface concentration, C_i^c, or critical temperature difference, ΔT^c, can be calculated from the constitutional supercooling criterion:

$$C_i^c m(K-1) = \Delta T^c = G L_s \tag{8}$$

For interfacial areas that have a concentration higher than the critical one, the interface is locally unstable (Fig. 5(a)). Thus the morphological instability cannot occur homogeneously but according to the acetone macrosegregation induced by fluid flow over the phase boundary, i.e., morphological instability is shaped by convective pattern that gives rise to localised microstructures predicted by Chen and Davis [4]. Consequently, precise information on the convective modes is extracted from spatio-temporal evolution of macroscopic shape of solidification front and from dynamics of propagation front of morphological instability, corresponding to the plan-cellular local transition at $C_i = C_i^c$ (Fig. 5(a)).

In our previous work [10], we observed two major cases on succinonitrile-0.2 wt% acetone alloy for velocities 1.4–1.8 $\mu m \cdot s^{-1}$ depending only initial crucible position: focus-like local microstructure around the centre of crucible for thick solid seed case or localised microstructure shaped by double-diffusive convective pattern for thin solid seed case (0.5 mm). In fact, initial crucible position changes

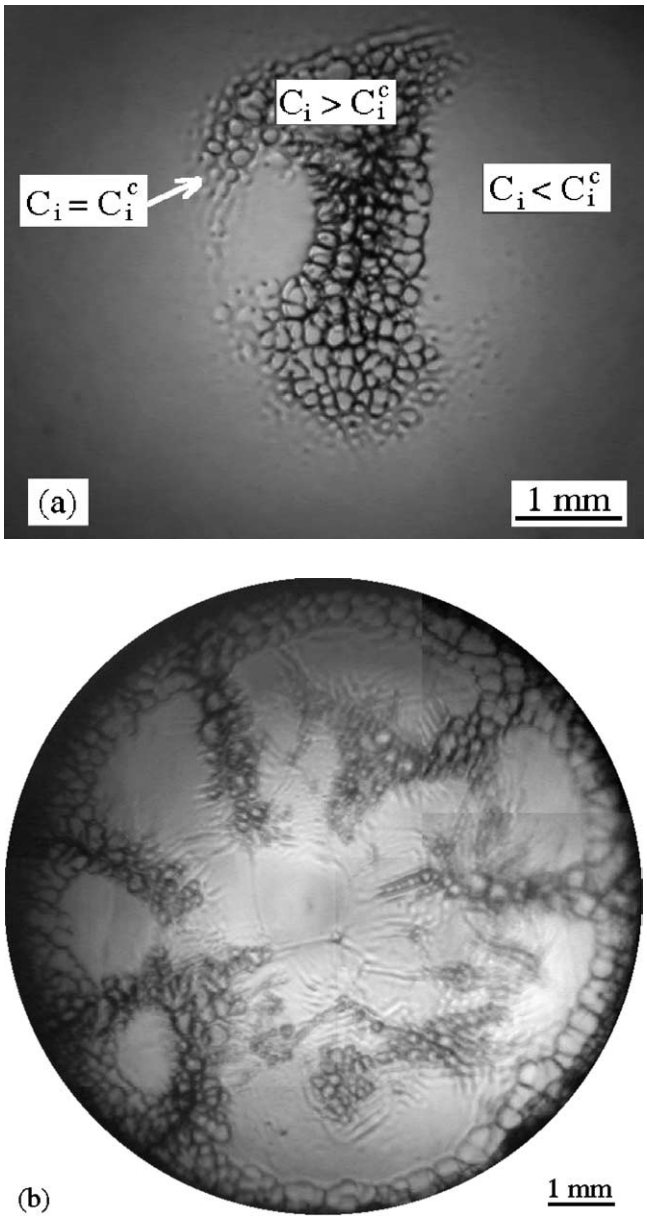

Fig. 5. Localised microstructure corresponding to different convective patterns, $V_p = 1.6$ µm·s^{-1}: (a) Thick solid seed, high thermal radial gradient; (b) Thin solid seed, weak radial thermal gradient: Double-diffusive cellular pattern.

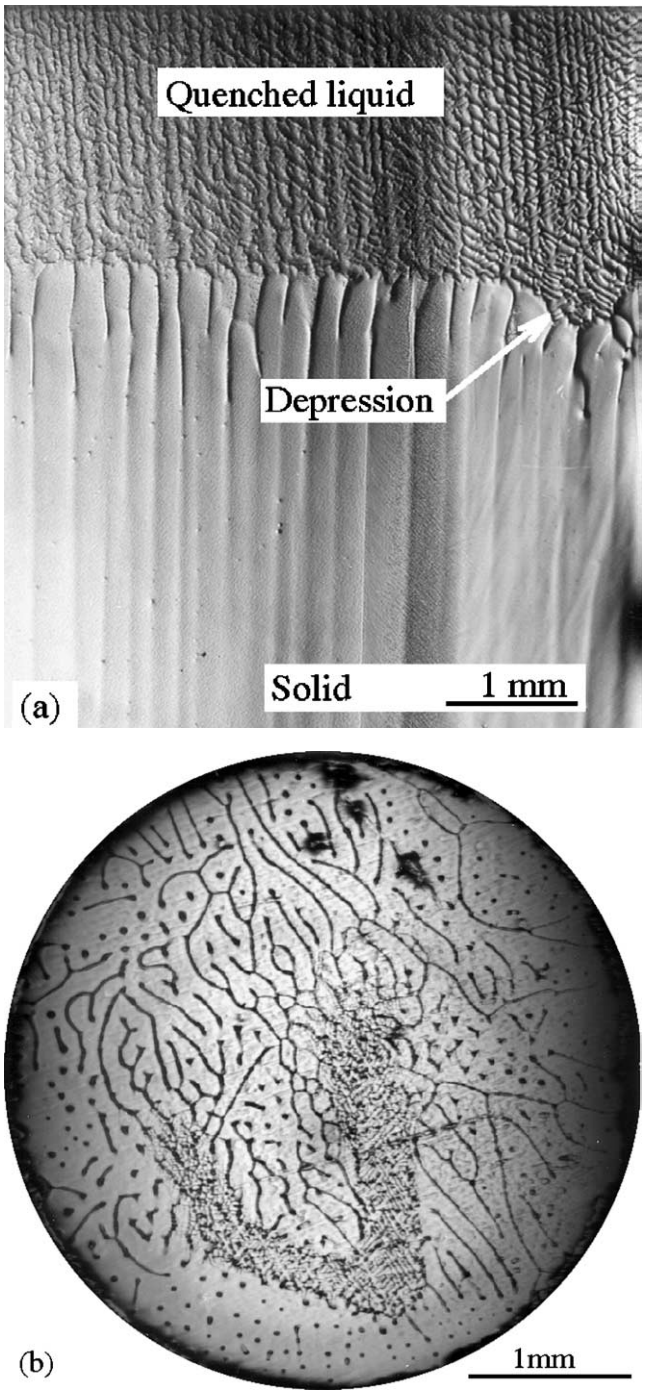

Fig. 6. Effect of double-diffusive convection on macroscopic shape of the interface. Homogeneous destabilisation of the interface (a) Longitudinal section, $\phi = 9.5$ mm, $V_p = 2.0$ µm·s^{-1}, $Ra_s/Ra_s^c = 1.0 \times 10^4$; (b) Transverse section, $\phi = 4$ mm, $V_p = 3.06$ µm·s^{-1}, $Ra_s/Ra_s^c = 2.9 \times 10^3$.

the value of initial thermal radial gradient due to the thermal exchanges between furnace and sample [18]. In case of a thin solid seed, the thermal radial gradient is negligible at the beginning of the solidification and double-diffusive convection may be dominant. That is why we frequently observe double-diffusive cellular pattern during the solidification initial transient. Fig. 5 represents other examples of localised microstructure on succinonitrile–acetone alloys.

Analogous results on lead-30 wt% thallium alloy are represented on the Fig. 6 for different sections. The longitudinal section shows the coexistence of different instabilities: morphological instability at 100 µm of scale and a depression at 1 mm of scale corresponding to the accumulation of solvent. Usually this depression has a form of a channel, visible on transverse cut of the sample in the solid–liquid interfacial region as a thin dendritic area corresponding quenched liquid (V shape on the Fig. 6(b)). The pattern formed by channels corresponds to the up-going part of double-diffusive convec-

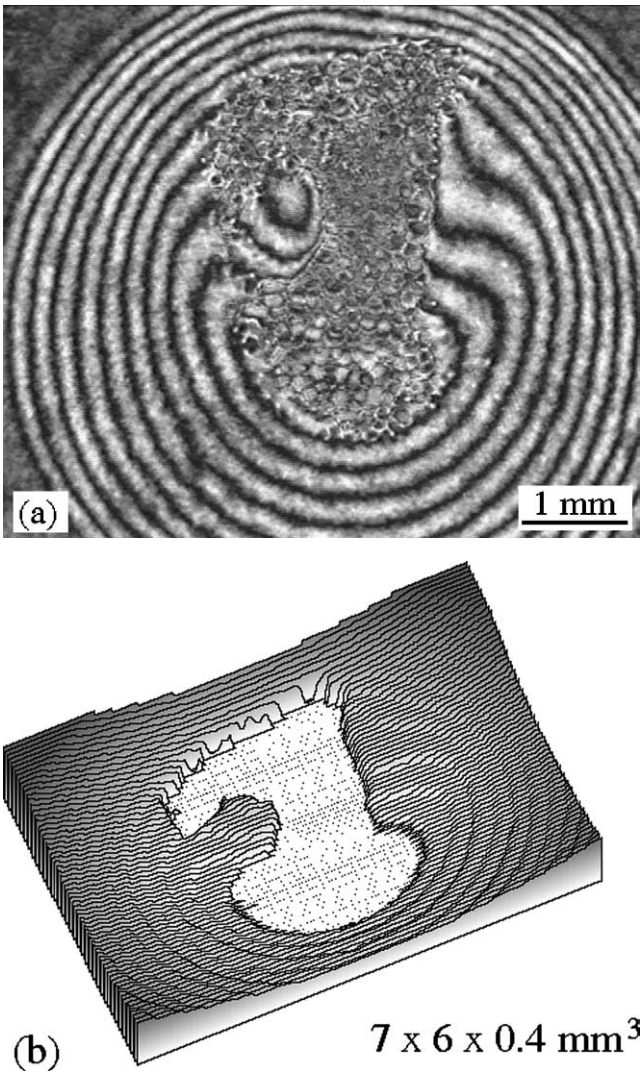

Fig. 7. (a) Interface interferogram and (b) its 3D representation corresponding to the case of Fig. 4(a). Negative thermal radial gradient.

tion [11,12]. In accordance with local equilibrium condition of the interface, the depression channel is a proof of the existence of the lateral solute gradient. Nevertheless, there is no propagation front of morphological instability, and no gradient on the level of morphological instability.

As we saw, both alloys exhibit similar double-diffusive instability. We should expect to observe localised microstructure for both alloys. However, we observed homogenous destabilisation of solid–liquid interface for lead-30 wt% thallium alloy, i.e., no localisation of the microstructure. The experiment in Fig. 6(b) is done in the region of "poxes" and "elongated cells" corresponding to morphological instability just above the threshold. Even near the threshold of morphological instability, we do not observe the coexistence of planar and destabilised interface morphology. The explanation of this difference is related to the parallelism of the liquidus and solidus curves (Fig. 1(b)). For a given velocity V, there is no unique critical concentration corresponding to

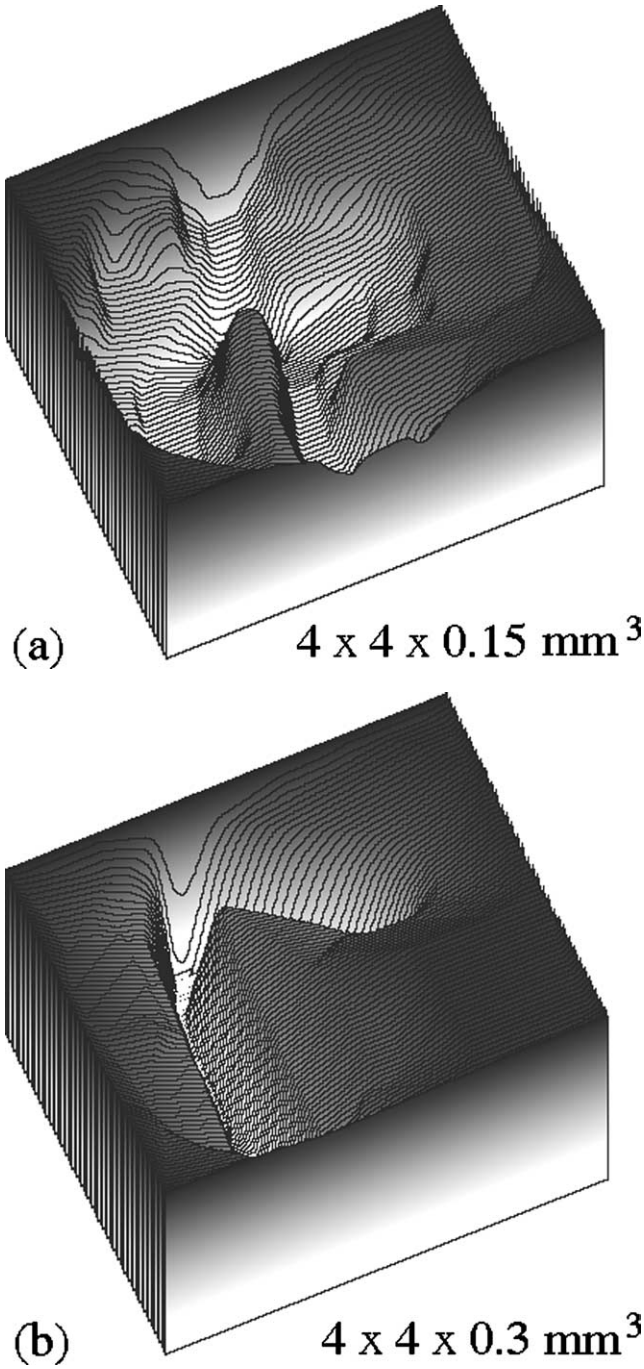

Fig. 8. 3D representation of solid–liquid interface for lead-30 wt% thallium alloy, $\phi = 4$ mm. Weak thermal radial gradient. Depression channels cross together (a) in the middle of crucible, $V_p = 1.14$ µm·s^{-1}, $Ra_s/Ra_s^c = 5.6 \times 10^4$, (b) at the border of the crucible, $V_p = 2.75$ µm·s^{-1}, $Ra_s/Ra_s^c = 4.0 \times 10^3$.

the ΔT^c, but a domain of concentration. Direct consequence of this fact is that, even if the convection induces a lateral concentration gradient, the level of morphological instability does not change. The fact that for the same velocity we have a range of critical concentration is shown in the transition curve of morphological instability $C_0(G/V_p)$ in Fig. 4

of [28]. Above 20 wt% thallium, the slope of this curve goes to infinity with concentration. This example shows that Chen and Davis prediction [4] is not available for alloys ΔT constant. As a rule, a particular attention will be taken for non-dilute alloy solidification, for which K and m are not constant.

For transparent alloys, there is a large contribution of the growth velocity to the level of thermal radial gradient. During initial transient of solidification, thermal radial and axial solute profiles progressively build up. The choice of convective mode in growth transient is strongly related to the dominant driving force during the formation of two profiles. Frequently, the effect of the radial temperature gradient becomes dominant in transient state, thus unstable area evolves into a disk-like local structure independently of initial conditions [10]. The case of negative thermal radial gradient corresponds to the up-going flow in the centre of crucible, the concave macroscopic shape of the interface and the localisation of the microstructure in the middle of crucible (Fig. 7).

For metallic alloys, the thermal radial gradient is due to the anisotropy of thermal conductibility at the interface (Table 1) and, in our experimental conditions, is independent of growth velocity. We observe, at the scale of the crucible, weakly concave interface and formation of depression channels, which cross together anywhere, either at the centre of crucible forming a star (Fig. 8(a)) or on the border of crucible forming a V shape (Fig. 8(b)). As the crucible diameter, $\phi = 4$ mm, is very small with respect to the wavelength at the threshold of double-diffusive instability, we do not observe complete double-diffusive cell. By changing the crucible diameter, we change the level of convection due to the thermal radial gradient [11,12]. In accordance, the macroscopic shape of the interface changes and becomes convex, corresponding to the positive thermal radial gradient. This creates a thermal axisymmetric convective mode, which is down-going in the centre of crucible and pushes the up-going solutal flow pattern all along the border of the crucible (Fig. 9). Thus, a big double-diffusive cell almost centred in the crucible is observed, corresponding to the closed depression channel near the border of crucible, a signature of the up-going double-diffusive flow [12]. Similar patterns are observed in Bénard–Marangoni convection for silicon oil partially heated [29].

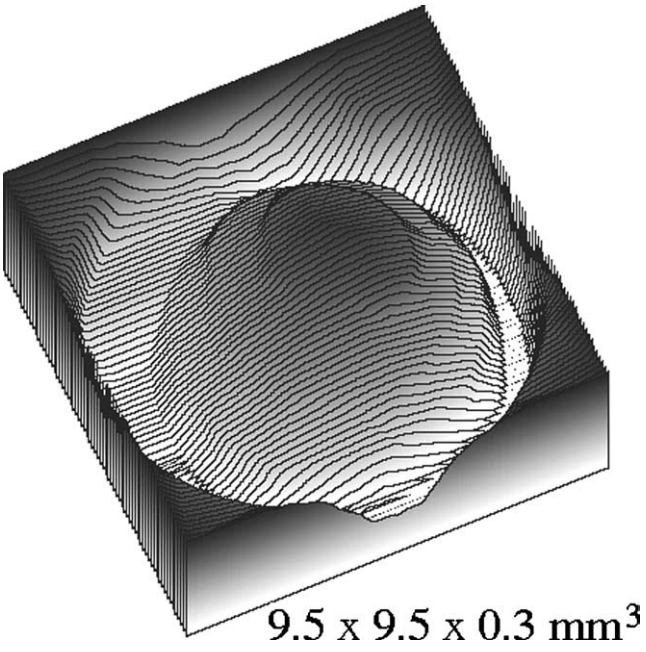

Fig. 9. 3D representation of solid–liquid interface for lead-30 wt% thallium alloy, $\phi = 9.5$ mm. Positive thermal radial gradient. Depression channel follows the crucible border. $V_p = 3.5\ \mu\text{m}\cdot\text{s}^{-1}$, $Ra_s/Ra_s^c = 1.9 \times 10^3$.

4. Conclusion

Localised microstructures due to the coupling effect of double-diffusive convective and morphological instabilities are observed for transparent alloys. However, for lead-30% thallium alloy, this coupling effect is not observed, because the level of morphological instability is independent of the concentration. This is due to the alloy characteristics (phase diagram), for which solidus and liquidus are parallel. The convection is thus a necessary but not a sufficient condition for the propagation front of morphological instability, for the lateral gradient on the level of morphological instability and for the localisation of the microstructure.

Two origins of convection are present simultaneously: radial thermal gradient and solute axial gradient. The domain of weak thermal radial gradient is experimentally difficult to obtain. It corresponds to the small diameter for lead–thallium alloys or the beginning of solidification in thin solid seed case for succinonitrile–acetone alloy. Observed double-diffusive cellular patterns are similar in both cases, and are related to the lateral confinement. Out of this domain (large diameter for lead–thallium alloys or thick solid seed case on succinonitrile–acetone alloys), there is a significant contribution of radial thermal gradient convection on the double-diffusive convective patterns. For positive thermal radial gradient case (lead–thallium alloys) a big double-diffusive cell, corresponding to the axisymmetric convective pattern is frequently observed. Consequently, flow is down-going in the centre of crucible. For negative thermal radial gradient case, (succinonitrile–acetone alloys), one o-ring axisymmetric convective pattern is observed up-going in the centre. In both cases, the convection due to the thermal radial gradient contributes to the arrangement of the double-diffusive pattern.

Acknowledgement

Financial and technical support from the Centre National d'Etudes Spatiales is gratefully acknowledged.

References

[1] S.R. Coriell, M.R. Cordes, W.J. Bottinger, R.F. Sekerka, Convective and interfacial instabilities during unidirectional solidification of a binary alloy, J. Cryst. Growth 49 (1980) 13–28.

[2] D.T.J. Hurle, E. Jakeman, A.A. Wheeler, Effect of solutal convection on the morphological stability of a binary alloy, J. Cryst. Growth 58 (1982) 163–179.

[3] B. Caroli, C. Caroli, C. Misbah, B. Roulet, Solutal convection and morphological instability in directional solidification of binary-alloys. 2. Effect of the density difference between the 2 phases, J. Phys. 46 (1985) 1657–1665.

[4] G.B. McFadden, R.G. Rehm, S.R. Coriell, W. Chuck, K.A. Morrish, Thermosolutal convection during directional solidification, Metall. Trans. A 15 (1984) 2125–2137.

[5] R.Z. Guerin, B. Billia, P. Haldenwang, Onset of solutal convection during directional solidification of a binary alloy in a cylinder, Phys. Fluids A 3 (1991) 1873–1879.

[6] J.J. Favier, A. Rouzaud, Morphological stability of the solidification interface under convective conditions, J. Cryst. Growth 64 (1983) 367–379.

[7] M. Hennenberg, A. Rouzaud, D. Camel, J.J. Favier, Morphological and thermosolutal instabilities inside a deformable solute boundary-layer during unidirectional solidification, J. Cryst. Growth 85 (1987) 49–58.

[8] S.N. Tewari, M.A. Chopra, Break-down of a planar liquid–solid interface during directional solidification; Influence of convection, J. Cryst. Growth 118 (1992) 183–192.

[9] Y.J. Chen, S.H. Davis, Flow-induced patterns in directional solidification: localized morphologies in three-dimensional flows, J. Fluid Mech. 421 (2000) 369–380.

[10] H. Jamgotchian, N. Bergeon, D. Benielli, Ph. Voge, B. Billia, R. Guérin, Localized microstructures induced by fluid flow in directional solidification, Phys. Rev. L. 87 (2001) 166105.

[11] H. Jamgotchian, B. Billia, L. Capella, Thermosolutal convection-induced morphologies of the solid–liquid interface during upward solidification of Pb-30wt% Tl alloys, J. Cryst. Growth 82 (1987) 342–350.

[12] H. Nguyen Thi, B. Billia, H. Jamgotchian, Influence of thermosolutale convection on the solidification front during upwards solidification, J. Fluid Mech. 204 (1989) 581–597.

[13] N. Noël, F. Zamkotsian, H. Jamgotchian, B. Billia, Optical device dedicated to the non-destructive observation and characterisation of the solidification of bulk transparent alloys in situ and in real time, Meas. Sci. Technol. 11 (2000) 66–73.

[14] H. Jamgotchian, B. Billia, L. Capella, Unidirectional growth of dilute Bi–Sb alloys, J. Cryst. Growth 62 (1983) 539–544.

[15] W.A. Tiller, K.A. Jackson, J.W. Rutter, B. Chalmers, The redistribution of solute atoms during the solidification of metals, Acta Met. 1 (1953) 428.

[16] W.W. Mullins, R.F. Sekerka, Stability of a planar interface during solidification of a dilute binary alloy, J. Appl. Phys. 35 (1964) 444–451.

[17] J.A. Warren, J.S. Langer, Prediction of dendritic spacings in a directional solidification experiment, Phys. Rev. E 47 (1993) 2702–2712.

[18] C.E. Chang, W.R. Wilcox, Control of interface shape in the vertical Bridgman–Stockbarger technique, J. Cryst. Growth 21 (1974) 135–140.

[19] C.E. Chang, V.F.S. Yip, W.R. Wilcox, Vertical gradient freeze growth of gallium arsenide and naphthalene: Theory and practice, J. Cryst. Growth 22 (1974) 247–258.

[20] S. Kaddeche, J.P. Garandet, C. Barat, H. Ben Hadid, D. Henry, Interface curvature and convection related macrosegregation in the vertical Bridgman configuration, J. Cryst. Growth 158 (1996) 144–152.

[21] C. Barat, T. Duffar, J.P. Garandet, Estimation of the curvature of the solid–liquid interface during Bridgman crystal growth, J. Cryst. Growth 194 (1998) 149–155.

[22] P. Haldenwang, R. Guerin, Transverse thermal effects in directional solidification, J. Cryst. Growth 244 (2002) 108–122.

[23] D.M.L. Bartholomew, A. Hellawell, Changes of growth conditions in the vertical Bridgman–Stockbarger method for the solidification of aluminum, J. Cryst. Growth 50 (1980) 453–460.

[24] R.J. Schaefer, S.R. Coriell, Convection-induced distortion of a solid–liquid interface, Met. Trans. A 15 (1984) 2109–2115.

[25] B. Caroli, C. Caroli, C. Misbah, B. Roulet, Solutal convection and morphological instability in directional solidification of binary-alloys, J. Phys. 46 (1985) 401–413.

[26] A.G. Ostrogorsky, G. Müller, A model of effective segregation coefficient, accounting for convection in the solute layer at the growth interface, J. Cryst. Growth 121 (1992) 587–598.

[27] N. Noël, H. Jamgotchian, B. Billia, In situ and real-time observation of the formation and dynamics of a cellular interface in a succinonitrile-0.5 wt% acetone alloy directionally solidified in a cylinder, J. Cryst. Growth 181 (1997) 117–132.

[28] H. Jamgotchian, B. Billia, L. Capella, Morphology of the solidification front during unidirectional growth of Pb–Tl alloys, J. Cryst. Growth 64 (1983) 338–344.

[29] O.V. Vashkevich, A.V. Gaponov-Grekhov, A.B. Ezerskii, M.I. Rabinovich, Solitary autostructures produced by thermal-convection in an inhomogeneously heated layer, Dokl. Akad. Nauk SSSR 293 (1987) 563–567.